Phonon Dispersion Relation of an Atomic Bose-Einstein Condensate

I. Shammass,[1] S. Rinott,[2] A. Berkovitz,[2] R. Schley,[2] and J. Steinhauer[2]

[1]*Department of Condensed Matter Physics, Weizmann Institute of Science, Rehovot 76100, Israel*

[2]*Department of Physics, Technion—Israel Institute of Technology, Technion City, Haifa 32000, Israel*

(Received 1 August 2012; published 5 November 2012)

We measure the time oscillations of a freely evolving standing wave of phonons in a Bose-Einstein condensate. We present the technique of short Bragg pulses, which stimulates the standing wave. The subsequent oscillations are observed *in situ*. The frequency of the oscillations gives the dispersion relation, the amplitude gives the static structure factor, and the decay gives the dephasing time. The new technique gives orders of magnitude more sensitivity than Bragg spectroscopy, allowing for the observation of deviations from the local density approximation. Specifically, it is seen that the phonons undergo a transition from three dimensions to one dimension, when their wavelength becomes longer than the transverse radius of the condensate. The one-dimensional regime contains an inflection point in the dispersion relation, a decrease in the superfluid critical velocity, a minimum in the group velocity, and an increase in the lifetime of the standing wave oscillations.

DOI: 10.1103/PhysRevLett.109.195301 PACS numbers: 67.85.De, 03.75.Kk, 05.30.Jp

Dispersion is the distortion of a wave packet due to the different velocities of each frequency component. A direct measurement of the phonon dispersion relation should therefore observe the oscillation frequency of the waves. Before the present work, the oscillation frequency was determined from a measurement of the energy of the quasiparticles, in an atomic [1–6] or exciton-polariton [7,8] condensate. Many of the previous measurements have employed Bragg spectroscopy [2,3], in which the condensate absorbs a predetermined momentum. The energy is adjusted to find the resonance condition, thus yielding a point on the excitation spectrum [4]. On the other hand, the energy can be determined by tomographic imaging [5]. In either case, the results were well described by the local density approximation (LDA) [2,9]. In this approximation, each point in the condensate is modeled as a homogeneous condensate, and a suitable average is taken over the inhomogeneous density of the actual condensate. Going beyond the LDA, various radial modes were resolved [6,10]. The present work introduces an alternative technique to Bragg spectroscopy, in which phonons are created with a predetermined momentum, and are allowed to freely evolve. The oscillation frequency is directly observed, thus obtaining a point on the dispersion relation.

This new technique is orders of magnitude more sensitive than Bragg spectroscopy. This results from heterodyne detection, in which the moving atoms composing the phonon interfere with the large condensate with population N. This amplifies the signal by approximately $\sqrt{N}$ relative to standard Bragg spectroscopy, in which the quasiparticles exit the condensate before being measured. An additional advantage of the new technique is that the frequency is determined from the zero crossing of the oscillation, rather than from the center of a broad peak in the Bragg response function. Furthermore, Bragg spectroscopy becomes difficult for small wave number k, because the quasiparticle cloud does not separate sufficiently from the condensate cloud in time-of-flight imaging. An analogous limitation occurs for exciton-polariton condensates [7,8]. In contrast, the phonons are best resolved for small k in our technique. The k range of our technique is thus complementary to that of Bragg spectroscopy.

In order to create the phonons, we present the technique of short Bragg pulses. The pulse employed is similar to that used in the Kapitza-Dirac effect [11], a phenomenon involving single particles rather than phonons. Two far-detuned laser beams with a relative angle θ impinge on the condensate for a short time τ, as shown in Fig. 1(a). The photons in the beams have a large energy uncertainty $\hbar\delta\omega$ which is on the order of $\hbar/\tau$. This allows the condensate to absorb a photon from either beam and emit a photon into the other, creating a phonon with energy $\hbar\omega_k$, as long as $\omega_k \ll 1/\tau$. The wave number k is precisely determined by θ. Counterpropagating phonons with well-defined k are thus produced, resulting in a standing wave.

During a short Bragg pulse, the energy in the phonons increases as $dE/dt = U^2tk^2N/2m$, where U is the amplitude of the sinusoidal potential resulting from the interference between the two laser beams, and m is the atomic mass [12]. This expression is independent of the frequency difference between the beams, due to the shortness of the pulse. Writing the energy in terms of the quasiparticle number, one obtains $N_{\mathbf{k}} = N_{-\mathbf{k}} = (U\tau/\hbar)^2 S_0(k)N/4$, where $S_0(k) = \hbar k^2/2m\omega_k$ is the zero-temperature static structure factor.

After the short Bragg pulse, the phonons freely propagate in the condensate. The wave function of a homogeneous condensate in the presence of phonons is given by [12,13]

$$\psi = (\psi_o + \delta\psi)e^{-i(\mu/\hbar)t}, \quad (1)$$

where μ is the chemical potential, and the small perturbation is given by

$$\delta\psi = \sum_{\mathbf{k}} \sqrt{\frac{N_{\mathbf{k}}}{V}}[u_k e^{i(\mathbf{k}\cdot\mathbf{r}-\omega_k t)} + v_k e^{-i(\mathbf{k}\cdot\mathbf{r}-\omega_k t)}],$$

where V is the volume of the condensate, and u_k and v_k are the Bogoliubov amplitudes, which were measured in Ref. [14]. We find that the density is given by

$$n = |\psi|^2 = n_0\left[1 + \frac{2}{\sqrt{N}}\sum_{\mathbf{k}}\sqrt{N_{\mathbf{k}}S_0(k)}\cos(\mathbf{k}\cdot\mathbf{r} - \omega_k t)\right], \quad (2)$$

where n_0 is the average density. For the standing wave, the Fourier transform of the density is given by

$$\rho_k = \left(\frac{U\tau}{\hbar}\right)NS_0(k)\sin(\omega_k t). \quad (3)$$

The standing wave is at a node just after the short Bragg pulse ($t = 0$), and we have adjusted the origin in time accordingly. Thus, by observing the frequency and amplitude of the oscillation of ρ_k, we obtain the dispersion relation ω_k, as well as $S_0(k)$.

The sinusoidal potential is created by imaging a spatial light modulator (SLM) onto the condensate. The SLM is illuminated by a far-detuned laser (803.5 nm). The image is filtered in the Fourier plane [15], resulting in two Bragg beams whose angle can be varied by changing the image on the SLM. The condensate is composed of ^{87}Rb atoms in the $F = 2$, $m_F = 2$ state and is confined in a cylindrically symmetric harmonic magnetic potential, with radial and axial frequencies of $\omega_\perp/2\pi = 224$ Hz and $\omega_z/2\pi = 26$ Hz, respectively. We primarily study a larger condensate with $\mu/h = 2340$ Hz, as well as a smaller condensate with $\mu/h = 1200$ Hz. Immediately after the short Bragg pulse, the density profile is very similar to the unperturbed condensate shown in Fig. 1(b), and in the integrated profile, Fig. 1(e). After a time corresponding to one-fourth of a period, however, the density modulation is at a maximum, as seen in Fig. 1(c). The density modulation disappears again after half a period, as seen in Fig. 1(d). In Figs. 1(b)–1(e), the only potential present is the harmonic trapping potential.

Figure 1(f) shows the magnitude squared of the Fourier transform of the profiles. The asterisk indicates the point corresponding to the applied k. We plot one phase component of this point as a function of time, as shown in Fig. 1(g). The phase is chosen to be that of the density modulation near the antinode [the solid black curve of Fig. 1(f)]. Since this measurement technique employs a predetermined spatial frequency k and is phase sensitive, it has the advantages of a lock-in amplifier [16].

The time of the zero crossing in Fig. 1(g) gives π/ω_k by Eq. (3). This time is determined by a linear fit to the data in the region of the zero crossing. Repeating the experiment for many values of k gives the dispersion relation ω_k, as shown in Fig. 2 for both values of μ. The error bars are too small to be seen for most points. Indeed, the errors are an order of magnitude smaller than the result for Bragg spectroscopy [4]. We have also made the perturbation to the condensate smaller, so the sensitivity improvement is actually more than an order of magnitude. The black curves of Fig. 2 are the result of a two-dimensional (2D) simulation of the Gross-Pitaevskii equation (GPE). This simulation is cylindrically symmetric with radial and axial coordinates. The agreement between the measured values and the simulation is excellent. The lowest measured

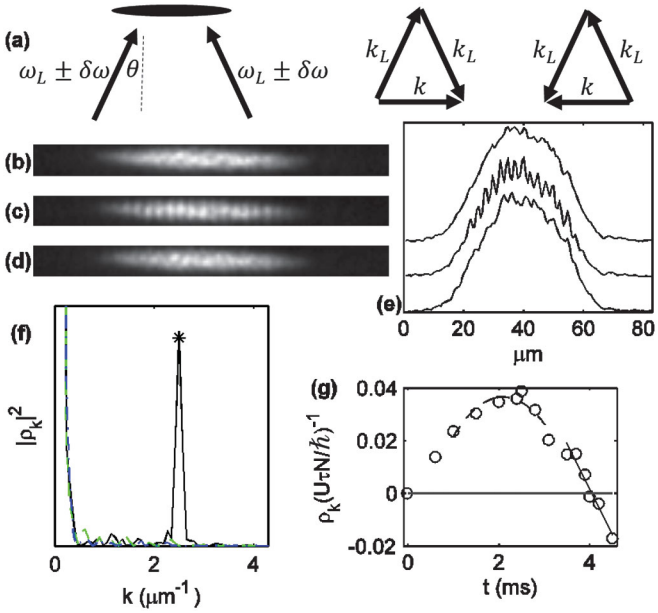

FIG. 1 (color). Creating a phonon standing wave by short Bragg pulses. The larger condensate is shown. (a) Two far-detuned laser beams, with frequency ω_L and wave number k_L, impinge on the condensate. Absorption from the left (right) beam and emission into the right (left) beam results in the production of a right-moving (left-moving) phonon with wave number k. The combination of the left- and right-moving phonons results in a standing wave. (b)–(d) Phase-contrast images of the *in situ* condensate, for a short 22 μsec Bragg pulse with $k = 2.47$ μm^{-1}, where (b) shows the time just before the pulse, (c) shows the first antinode of the standing wave, at 250 μsec and (d) shows the second node, at 510 μsec. (e) Integrated profiles of the images. The top, middle, and bottom curves correspond to (b), (c), and (d), respectively. The top and middle curves have been shifted vertically for clarity. (f) The magnitude squared of the Fourier transform of the profiles. The blue dash-dotted, black solid, and green dashed curves correspond to before the pulse, the antinode, and the node, respectively. The asterisk indicates the k value corresponding to the standing wave. (g) The time dependence of the Fourier transform of the standing wave, for $k = 0.35$ μm^{-1}. The linear fit at the zero crossing determines ω_k (solid line). The parabolic fit at the maximum determines $S_0(k)$ (dashed curve).

frequency is seen to be 80 Hz. Since this is much greater than the axial trap frequency of 26 Hz, discrete axial modes can be neglected [17]. Figure 2 also shows the local density approximation, which agreed well with previous measurements of the excitation energy [2–5].

In Fig. 2 it is seen that both the measured and simulated dispersion relations are depressed relative to the LDA curve near $k = 1\ \mu\mathrm{m}^{-1}$. This is particularly visible for the larger value of μ. This is emphasized in the upper inset, which shows the ratio between the dispersion relations. The ratio is clearly below unity in this k regime. Here, the depression in the dispersion relation is below a transition from three dimensions to one dimension (3D-1D transition) which occurs when the wavelength becomes longer than the transverse radius of the condensate. This result can be understood in terms of the discretization of the modes in the transverse (radial) direction. The broad LDA frequency spectrum is actually divided into narrow radial modes [6,10]. For small k, the LDA linewidth becomes sufficiently narrow that only a single radial mode is excited [6], giving the phonons a one-dimensional (1D) character. Equating the LDA linewidth $\delta\omega_k \approx 0.6\omega_k$ (FWHM) [9] with the spacing between radial modes of approximately $2\omega_\perp$ [6,10], a single mode will be excited for

$$\lambda > 0.9R_\perp, \tag{4}$$

where λ is the phonon wavelength, and $R_\perp$ is the Thomas-Fermi radius of the condensate perpendicular to the direction of propagation. The single mode excited in this frequency regime does not necessarily have the same frequency as the average over the LDA line shape. Thus, the measured dispersion relation deviates from the LDA curve. Not surprisingly, the depression in the dispersion relation can be seen in simulations of the lowest radial mode [6,10]. The inequality of Eq. (4) is indicated by the arrow in the upper inset of Fig. 2, which is seen to agree with the regime of the depression in the dispersion relation. As an additional verification that the transition is associated with the transverse degree of freedom, we perform a 1D GPE simulation of the experiment. We compare the results of this simulation with a 1D LDA average, as indicated by the dotted line in the upper inset of Fig. 2. It is seen that the simulation always agrees with the LDA, since there are no transverse modes present.

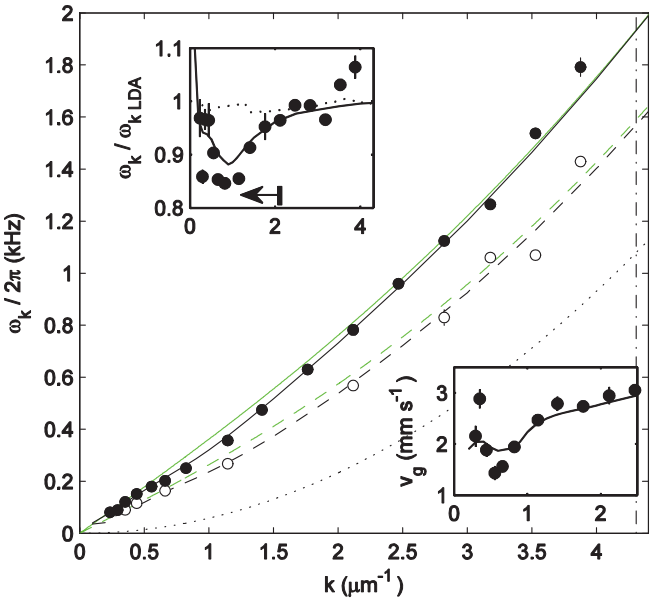

FIG. 2 (color). The phonon dispersion relation of a Bose-Einstein condensate. The filled (open) circles indicate $\mu/h =$ 2340 Hz (1200 Hz). The error bars (which are too small to be seen for most points) indicate the standard error of the mean. The black curves indicate the result of the 2D GPE simulation. The green curves are the LDA approximation. Solid (dashed) curves correspond to the larger (smaller) value of μ. The dotted curve is the free-particle spectrum $\omega_k = \hbar k^2/2m$. The dash-dotted line indicates the inverse healing length, the maximum k of the phonon regime, for the larger value of μ. The upper inset shows the ratio between the dispersion relation and the LDA approximation for the experiment (filled circles), the 2D GPE simulation (solid curve), and the 1D GPE simulation (dotted curve), for the larger value of μ. The arrow indicates the 1D regime. The lower inset shows the group velocity for the experiment (filled circles) and the 2D GPE simulation (solid curve), for the larger value of μ. The group velocity is computed from the dispersion relation by a 3-point derivative.

According to the Landau criterion [1], the depression in the dispersion relation corresponds to a slight decrease in the superfluid critical velocity. At the depression, $\omega/k = 1.91 \pm 0.01$ mm sec^{-1}, which is the lowest value for the entire measured dispersion relation, and thus corresponds to the critical velocity. For the LDA, ω/k is smallest for $k = 0$, and takes the value 2.22 mm sec^{-1}. Thus, the critical velocity is suppressed to 0.9 of its LDA value, due to the 1D nature of the phonons. The depression also implies a minimum in the group velocity $v_g = d\omega/dk$, as seen in the lower inset of Fig. 2. In superfluid helium, the minimum in the group velocity corresponds to a roton [1,18], an excitation whose wavelength is on the order of the effective hard-sphere radius of the atoms [19]. Here the minimum is weaker, and the relevant length scale is the transverse radius of the condensate.

The oscillation amplitude in Fig. 1(g) gives $S_0(k)$ by Eq. (3). This value is determined by a parabolic fit in the region of the maximum. The result is shown in Fig. 3. The experimental values in Fig. 3 have been multiplied by a factor of 1.5, in order to agree with the 2D GPE simulation for low k. This factor is probably required due to uncertainty in the intensity of the Bragg beams at the location of the condensate, which affects U in Eq. (3). For small k, the functional agreement with the simulation is very good. The uncertainty expressed by the error bars is seen to be an order of magnitude improvement relative to the Bragg spectroscopy results in this regime [4]. However, for larger k, the measured values roll off due to the finite resolution of the imaging system, which decreases the apparent values of ρ_k.

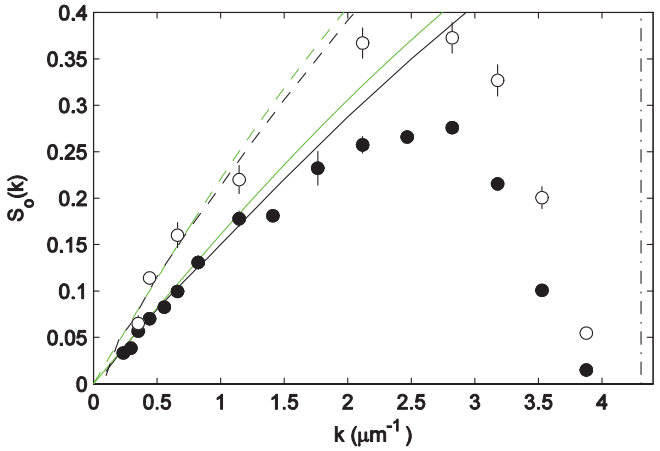

FIG. 3 (color). The static structure factor. The filled (open) circles indicate $\mu/h = 2340$ Hz (1200 Hz). The error bars indicate the standard error of the mean. The black curves indicate the result of the 2D GPE simulation. The green curves are the LDA approximation. Solid (dashed) curves correspond to the larger (smaller) value of μ. The dash-dotted line indicates the inverse healing length for the larger value of μ.

We now explore the decay of the oscillations, as seen in Fig. 4(a). The short Bragg pulse (as with any Bragg pulse) excites several Bogoliubov modes which subsequently dephase, causing the decay. The filled circles of Fig. 4(b) show the Q factor of the oscillations, the number of radians $\omega_k t$ required for the amplitude to decay by $1/\sqrt{e}$. It is seen that for long wavelengths, Q increases significantly. This is in contradiction to the LDA prediction for the decay, which is due to the dephasing of the oscillations at various locations in the condensate. For small k, the LDA linewidth implies a constant Q of $1/0.6$, as indicated by the dashed line in Fig. 4(b). We can make a more precise LDA prediction by extending the LDA to include the time dependence of the density. Writing Eq. (2) for the standing wave, and taking the various quantities to be functions of position,

$$n(\mathbf{r}, t)_{\mathrm{LDA}} = n_0(\mathbf{r})\Big[1 + \Big(\frac{U\tau}{\hbar}\Big)S_0(\mathbf{r}, k)\{\sin[kx - \omega_k(\mathbf{r})t] - \sin[kx + \omega_k(\mathbf{r})t]\}\Big], \quad (5)$$

where x is the direction of oscillation of the standing wave, and we have adjusted the time origin to form a node at $t = 0$. By Eq. (5), each point in the condensate oscillates with a different frequency and amplitude, depending on the local density. The density profile and its Fourier transform ρ_k is computed for Eq. (5), yielding the solid curve in Fig. 4(b). Again it is seen that the measured Q significantly exceeds the LDA prediction for small k. The discrepancy between the measurement and the LDA is due to the 3D-1D transition. In the 1D regime, the single radial mode has a much narrower linewidth than the LDA, resulting in larger

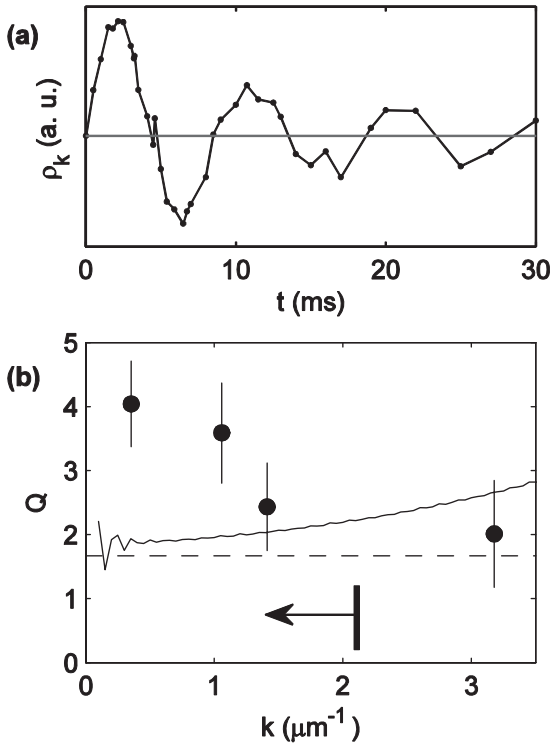

FIG. 4. The decay of the phonon standing wave. The larger condensate is shown. (a) The amplitude of the standing wave as a function of time, for $k = 0.35$ μm^{-1}. (b) The Q of the oscillation. The error bars reflect the uncertainty due to the finite number of cycles measured. The solid curve is the LDA result, by Eq. (5). The dashed line is the LDA result for small k. The arrow indicates the 1D regime.

Q. This regime is indicated by the arrow in Fig. 4(b). It is seen that the arrow approximately corresponds to the region in which the measured values display increased Q.

In conclusion, we have studied the time evolution of phonons in a Bose-Einstein condensate, thus obtaining the dispersion relation, the static structure factor, and the previously inaccessible dephasing time. The phonon standing wave is stimulated by the novel technique of short Bragg pulses. The sensitivity of the measurement is more than an order of magnitude beyond the previous state of the art. Furthermore, the *in situ* technique is particularly suitable for studying long wavelengths. These advancements allow for the observation of a 3D-1D transition. In the 1D regime corresponding to long wavelengths, the phonons are characterized by a single radial mode. This mode has a lower frequency and longer lifetime than predicted by the local density approximation. The 1D regime results in a decreased superfluid critical velocity, and a minimum in the group velocity. The 1D nature of the long-wavelength modes is important for the analysis of sonic black holes [20–25].

We thank Chris Westbrook and Nadav Katz for helpful comments. This work was supported by the Israel Science Foundation.

[1] Ph. Nozières and D. Pines, *The Theory of Quantum Liquids* (Addison-Wesley, Reading, MA, 1990), Vol. II, Chap. 1–3, 5, and 9.
[2] D. M. Stamper-Kurn, A. P. Chikkatur, A. Görlitz, S. Inouye, S. Gupta, D. E. Pritchard, and W. Ketterle, Phys. Rev. Lett. **83**, 2876 (1999).
[3] J. Stenger, S. Inouye, A. P. Chikkatur, D. M. Stamper-Kurn, D. E. Pritchard, and W. Ketterle, Phys. Rev. Lett. **82**, 4569 (1999).
[4] J. Steinhauer, R. Ozeri, N. Katz, and N. Davidson, Phys. Rev. Lett. **88**, 120407 (2002).
[5] R. Ozeri, J. Steinhauer, N. Katz, and N. Davidson, Phys. Rev. Lett. **88**, 220401 (2002).
[6] J. Steinhauer, N. Katz, R. Ozeri, N. Davidson, C. Tozzo, and F. Dalfovo, Phys. Rev. Lett. **90**, 060404 (2003).
[7] S. Utsunomiya, L. Tian, G. Roumpos, C. W. Lai, N. Kumada, T. Fujisawa, M. Kuwata-Gonokami, A. Löffler, S. Höfling, A. Forchel, and Y. Yamamoto, Nat. Phys. **4**, 700 (2008).
[8] V. Kohnle, Y. Léger, M. Wouters, M. Richard, M. T. Portella-Oberli, and B. Deveaud-Plédran, Phys. Rev. Lett. **106**, 255302 (2011).
[9] F. Zambelli, L. Pitaevskii, D. M. Stamper-Kurn, and S. Stringari, Phys. Rev. A **61**, 063608 (2000).
[10] C. Tozzo and F. Dalfovo, New J. Phys. **5**, 54 (2003).
[11] P. L. Gould, G. A. Ruff, and D. E. Pritchard, Phys. Rev. Lett. **56**, 827 (1986).
[12] L. Pitaevskii and S. Stringari, *Bose-Einstein Condensation* (Oxford University, New York, 2003), Chap. 5 and 12.
[13] E. M. Lifshitz and L. P. Pitaevskii, in *Statistical Physics*, edited by L. D. Landau and E. M. Lifshitz, Course of Theoretical Physics Vol. 9 (BPCC Wheatons Ltd., Exeter, Great Britain, 1991), Part 2, Sec. 30.
[14] J. M. Vogels, K. Xu, C. Raman, J. R. Abo-Shaeer, and W. Ketterle, Phys. Rev. Lett. **88**, 060402 (2002).
[15] A. Itah, H. Veksler, O. Lahav, A. Blumkin, C. Moreno, C. Gordon, and J. Steinhauer, Phys. Rev. Lett. **104**, 113001 (2010).
[16] N. Katz, R. Ozeri, J. Steinhauer, N. Davidson, C. Tozzo, and F. Dalfovo, Phys. Rev. Lett. **93**, 220403 (2004).
[17] W.-C. Wu and A. Griffin, Phys. Rev. A **54**, 4204 (1996).
[18] R. P. Feynman, Phys. Rev. **94**, 262 (1954).
[19] J. Steinhauer, R. Ozeri, N. Katz, and N. Davidson, Phys. Rev. A **72**, 023608 (2005).
[20] W. G. Unruh, Phys. Rev. Lett. **46**, 1351 (1981).
[21] O. Lahav, A. Itah, A. Blumkin, C. Gordon, S. Rinott, A. Zayats, and J. Steinhauer, Phys. Rev. Lett. **105**, 240401 (2010).
[22] L. J. Garay, J. R. Anglin, J. I. Cirac, and P. Zoller, Phys. Rev. Lett. **85**, 4643 (2000).
[23] J. Macher and R. Parentani, Phys. Rev. A **80**, 043601 (2009).
[24] R. Balbinot, A. Fabbri, S. Fagnocchi, A. Recati, and I. Carusotto, Phys. Rev. A **78**, 021603(R) (2008).
[25] P.-É. Larré, A. Recati, I. Carusotto, and N. Pavloff, Phys. Rev. A **85**, 013621 (2012).